ORIGINAL PAPER

A geospatial analysis of land use dynamics and its impact on land surface temperature in Siliguri Jalpaiguri development region, West Bengal

Ivana Hoque[1] · Smt. Kabita Lepcha[2]

Abstract

Urbanization associates physical expansion of built up land which influences rapid change of land use/landcover (LULC) pattern of an area. LULC is one of the most visible results of modification of the natural features by human interventions which leads to encroachment of natural land and related degradation. The present paper relates to the exploration of remote sensing and geographic data to study the land use patterns, land cover classification, relationship between different LULC parameters and their impacts. GIS and remote sensing have been integrated as vital tool for the analysis and investigation of spatio temporal data. Siliguri Jalpaiguri planning region has been growing very rapidly over the last decades that brings great changes in the nature of land use pattern and related transformation. The result indicates 0.34 °C increase of land surface temperature per year and its association with spatial indices such as Normalized Difference Vegetation Index, Normalized Difference Water Index, and Normalized Difference Built Up Index.

Keywords Land use landcover pattern · Land transition · Land surface temperature · Spatial indices · Urban temperature

Introduction

The wide availability of the Landsat data has been extensively used in land use/cover classification and change detection at regional scales (Weng 2001, 2002; Mubea and Menz 2012; Turner et al. 1994). Urbanization process brings changes in land use pattern resulting in significant environmental impacts (Xiao et al. 2002). Land use land cover change by urbanization process, especially the transformation of natural land to urban uses, is the most significant form of global environmental change (Briassoulis 2000). One of the major impacts of LULC change driven by urbanization is the change in land surface temperature (LST) which is closely related with

different LULC parameters. Increase of LST gives rise to urban heat island which is a worldwide concerning phenomenon in the cities at present. For controlling the land surface temperature, major influencing factors are the characteristics of surface cover, urban morphology, and anthropogenic activity.

The rapid population growth in urban areas creates pressure on the natural environment and on its resources. As a result, the land use pattern and land cover of the surface change rapidly. This type of scenario is mostly being seen in developing countries as well in India (Mohan et al. 2011). The environmental degradation is not only the result of population growth actually; it is the product of population, energy, industrialization, and urbanization (Bowler et al. 2010). Studies have carried out for evaluating the rise in urban temperature and formation of urban heat islands in the cities of world (Liu and Weng 2008; Ayanlade and Howard 2019). Due to increasing population and infrastructure for rapidly growing urban areas, the urban heat islands (UHIs) have been developed (Sobrino et al. 2004). All cities in India have been experiencing this ongoing phenomenon involving large scale land use changes with globalization (Ramachandra et al. 2012; Mallick and Rahman 2012). Recent studies found out the rapid changes in the land use and land cover of a region which has become a major environmental issue in India (Mohan et al. 2011). The

✉ Ivana Hoque
   Ivana01102009@gmail.com

   Smt. Kabita Lepcha
   Kabitaugb@gmail.com

1   Research Scholar, University of Gour Banga, Malda, West Bengal, India

2   Department of geography, University of Gour Banga, Malda, West Bengal, India

study by Ramachandra clearly shows that the rate of increase in the urbanization leads to change in the land surface temperature. The increase in the temperature is in the range of 3 to 4 °C during 1989 to 2010 in India. The studies by Bowler et al. (2010); Afzan Buyadi et al. (2013) point out that temperature increase can lead to unsustainable development with the reduction of green spaces and also changes in local climate and formation of UHIs.

Fast urbanization in Siliguri Jalpaiguri planning area (SJDA) has been noticed from post independence which has played a significant and key role in the urbanization and development process of West Bengal. Majority of studies based on land use parameters and urbanizations have focused on mega cities of India while very less importance has been given to urban entities of north of West Bengal. SJDA has emerged as the third largest urban agglomeration in West Bengal just after Kolkata and Asansol-Durgapur with 83.65% decadal urban growth rate. This population outgrowth and accelerating urban land have triggered the land cover conversion rapidly to accommodate the need for residential area over the time. A rational and comprehensive strategy for the land use planning and urban environment within a regionally and ecologically sustainable framework has become an absolute necessity in developmental process of the region.

The present study attempts to explore three objectives: (I) To assess the changing pattern of land use in the Siliguri Jalpaiguri planning region, focusing on land conversion of urban areas, (II) to show the relationship between land use land cover and various spatial indices, and (III) to assess the environmental impact of urbanization with reference to reduction of green space and increase of land surface temperature. In order to reach the objectives, the present study has employed statistical, geospatial tools, and indices. Studies have been carried out to explore the relationship between different land use indices through RS and GIS technology. For this purpose, Normalized Difference Vegetation Index (NDVI by Carlson and Ripley 1997; Purevdorj et al. 1998), Normalized Difference Built Up index (NDBI by Zha et al. 2003), and Modified Normalized Difference Water Index (MNDWI by Xu 2006), etc were formulated to show spatial distribution of different LULC types and their relationships. Monitoring and management of land use dynamics would help in land use planning by bridging the knowledge gap between present and past and mitigation of environmental impacts.

Study area

The Siliguri Jalpaiguri Development Area (SJDA) is located (Fig. 1) in the northern part of West Bengal comprising components of two districts, Darjeeling and Jalpaiguri. The southern part of Darjeeling district and the adjacent western part of

Jalpaiguri district define the formation of the SJDA. The surrounding hinterland of the area comprises the whole of North Bengal including the five district of Darjeeling, Coochbihar, Jalpaiguri, Malda, and Dinajpur. Physiographically, Siliguri Jalpaiguri Development area may be divided into three divisions: hills, piedmont, and plains. The SJDA zone mostly lies under the piedmont zone with the major central southern part being "Terai-Dooars" and the northern part comprising of alluvial fans old terraces. A very small component of "active plain" zone exists at the south-eastern part of SJDA within Jalpaiguri district.

The study area covers four blocks of Darjeeling district namely Matigara, Naxalbari, Phansidewa, and Khoribari and four blocks of Jalpaiguri districts namely Jalpaiguri, Rajganj, Mal, and Mainaguri. The study area consists of one Municipal Corporation and two municipalities which are Jalpaiguri municipality and Mal municipality. The area includes 23 census towns, 14 in Darjeeling district and 9 in Jalpaiguri district and 540 revenue villages. The land area under the jurisdiction of SJDA is 2658 km^2 after the recent inclusion of Mal and a portion of Mainaguri CD block consisting 14 villages. In the census year 2011, the total population of SJDA was 2.37 million, out of 1.28 is rural and 1.09 million populations is urban. The region is growing fast characterized by combined effect of demographic and spatial dynamics (Fig. 1).

Data base and methodology

Landsat imagery is particularly helpful in monitoring land use change detection as it provides an efficient support for wide landscape analysis and such data is regularly updated and easily accessible (Nkeki 2016). The data utilized in this study are cloud-free multi-temporal and multi-spectral Landsat TM (Thematic Mapper) data for 1991, 2001, and Landsat 8 OLI (Operational Land Imager) data for 2017. These satellite data have obtained from USGS GLOVIS (United States Geological Survey Global Visualization Viewer) website to analyze the land use land cover pattern. Specification of the satellite data has provided below (Table 1).

Image processing and classification

The obtained Landsat data of two path/row series were mosaicked to extract the study area in a single image with the help of Arc GIS 10.3.1 software. Then the images were georeferenced to UTM 45° N WGS-84 datum for supervised classification and necessary output generation. The methodology of the present analysis can be divided into three stages: generation of land use/land covers map, derivation of spatial indices, and assessment and determination of the relationship between LST and other land use parameter. The whole

Fig. 1 Location of the study area within West Bengal and within Darjeeling, Jalpaiguri District
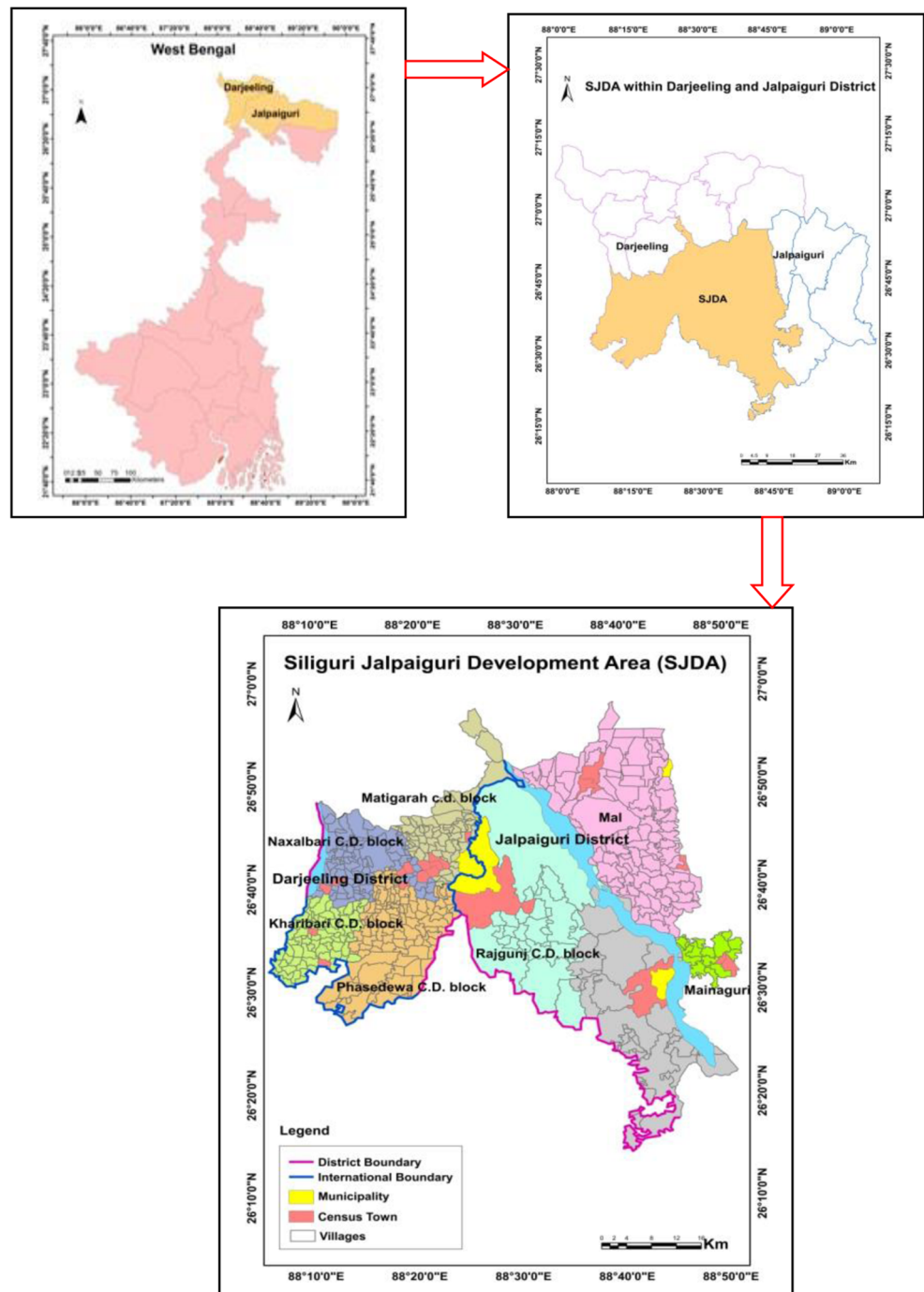
methodological process adopted in the study has been summarized in below-listed diagram (Fig. 2).

Using the Landsat images of three temporal periods, a combination of supervised classification was performed in the ArcGIS 10.3 software for deriving land use layers. The land use categories included forest, light vegetation cover, agricultural plantation, construction land, cultivated land, water, and waste land. Information has been extracted with the use of GIS for land use analysis to detect the changes in the vast expanse of land cover of the study region.

Accuracy assessment of the classified images has been made through Kappa coefficient to validate the post classification analysis. More than 300 reference points were generated on 1991 and 2017 land use map for assessing user's accuracy, producer's accuracy, overall accuracy, and Kappa coefficient. Selected points were superimposed on the classified images to characterize the underlying pixel or land use types of each point which were compared with the existing ground characteristics using Google archive data. Kappa coefficient is one of the most reliable accuracy indicators (Foody 1992; Ma

Table 1 Characteristic of Landsat satellite images used in this study

Satellite	Sensor ID	Year	Acquisition date	Resolution	Path/row	Projection
Landsat 5	TM	1991	January 8, 1991	30 m	139/41139/42	UTM-WGS1984
Landsat 5	TM	2001	January 19, 2001	30 m	139/41139/42	UTM-WGS1984
Landsat 8	OLI_TIRS	2017	December 01, 2017	30 m	139/41139/42	UTM-WGS1984

Source: earth explorer USGS

For Landsat TM 5 band-6 and for Landsat OLI imagery band 10 and 11 are used to derive LST. Red band 3 for TM, 4 for OLI and near-infrared band 4 for TM, band 5 for OLI are used for generating NDVI

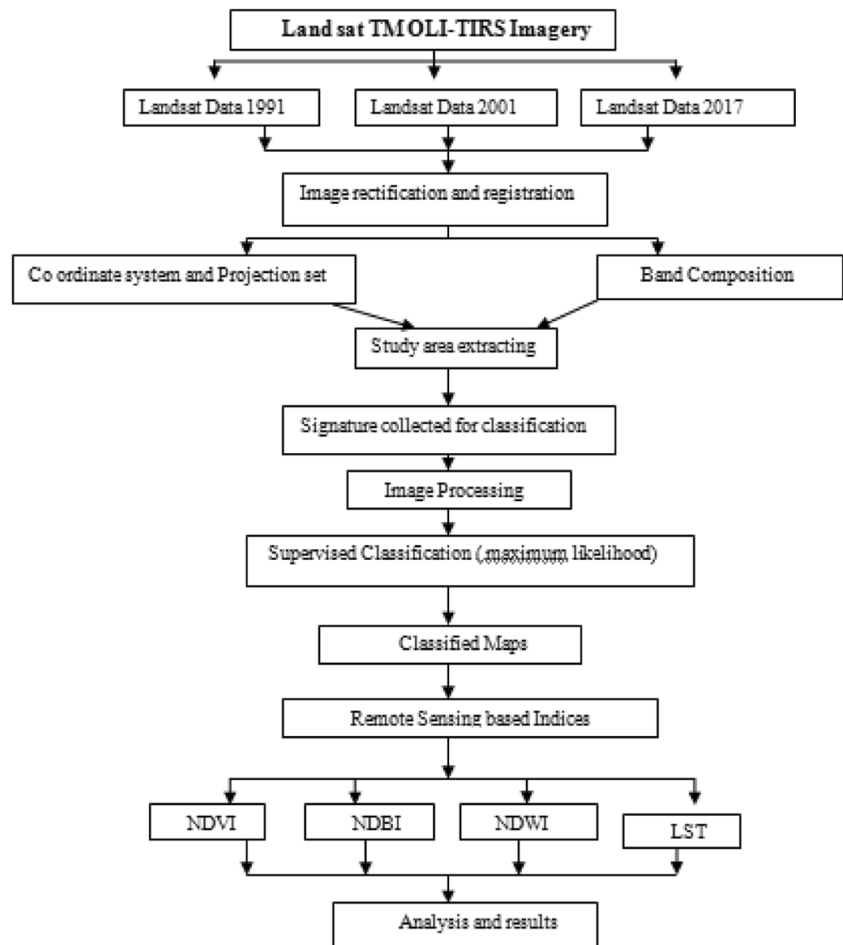and Redmond 1995). Kappa coefficient (K) value is computed by the following Cohen's formula:

$$K = \frac{\sum \frac{a}{N} - \sum \text{ef}}{1 - \sum \text{ef}} \tag{1}$$

where a is the sum of diagonal frequency, N is the total number of data, and ef is the expected frequency.

Expected frequency (ef) can be calculated using the following formula:

$$\text{ef} = \frac{\text{Row total} \times \text{Column total}}{N} \tag{2}$$

Fig. 2 Flow diagram of methodological proceeding

Coefficient value closer to 1 produces perfect agreement between the classified image and referenced image which signifies highest number of correctly classified pixels.

Method of derivation of land surface temperature (LST)

Land surface temperature (LST) of SJDA and its urban area is quantitatively derived from Lantsat TM 5 for the year 1991 and 2001 and Landsat 8 OLI (Operational Land Imager) imagery for the year 2017 having 0% cloud cover. These images of different sensors have different thermal bands such as for

Table 2 Accuracy assessment of land use land cover map of 1991 from Landsat TM data

Land use class	F	L.V	T.G	A.L	B.U	W.B	W.L	Row total	User's accuracy
F	55	2	1	0	0	2	0	60	91.60%
L.V	2	34	1	1	0	2	1	40	85%
T.G	1	0	52	3	1	1	1	60	86.70%
A.L	0	1	3	32	1	3	2	42	76.20%
B.U	0	0	1	1	48	0	0	50	88.90%
W.B	2	2	1	3	0	46	0	54	85.20%
W.L	0	1	1	2	0	0	26	30	86.60%
Column total	60	40	60	42	50	54	30	336	
Producer's accuracy	91.60%	85%	86.60%	76.20%	96%	85.20%	86.70%		
Overall accuracy					87.20%				
Kappa coefficient					0.845				

Diagonal italic values represent correctly classified samples for each land use class. *F* forest, *L.V* light vegetation, *T.G* tea garden, *A.L* agricultural land, *B.U* built up, *W.B* water body, *W.L* waste land

Landsat TM 5 band-6 is thermal band, and Landsat OLI imagery provides 11 bands in which band 10 and band 11 are thermal bands. Derivation of temperature from TM and OLI imageries follows different steps in converting digital values into spectral radiance which are discussed below:

Step 1: Conversion of band 6 digital values to spectral radiances from Landsat TM 5.

To convert the band 6 digital values into radiance values $(L\lambda)$, the following formula has been used (Landsat Project Science Office 2002):

$$L\lambda = \frac{LMAX\lambda - LMIN\lambda}{QCALMAX - QCALMIN} \times (QCAL - QCALMIN) + LMIN\lambda \tag{3}$$

where $L\lambda$ is the atmospherically corrected cell value as radiance, QCAL is the digital value of imagery, LMINλ is the spectral radiance scales to QCALMIN, LMAXλ is the spectral radiance scales to QCALMAX, QCALMIN is the minimum quantized calibrated pixel value (typically 1), and QCALMAX is the maximum quantized calibrated pixel value (typically 255).

Conversion of band 10 and 11 digital values to spectral radiances from Landsat OLI.

To convert the band 10 and 11 digital values of Landsat OLI, the following formula has been used:

$$L\lambda = ML \times QCAL + AL \tag{4}$$

where $L\lambda$ is the TOA (top of atmosphere) spectral radiance, ML is the radiance multi band X, AL is the radiance add band X, Qcal is the quantized and calibrated standard product pixel value, and X is the band number.

Here ML and AL are band-specific multiplicative rescaling factor and band-specific additive rescaling factor respectively, acquired from metadata file (MTL file).

Table 3 Accuracy assessment of land use land cover map of 2017 from Landsat OLI data

Land use Classes	F	L.V	T.G	A.L	B.U	W.B	W.L	Row total	User's accuracy
F	57	0	1	0	0	2	0	60	95%
L.V	1	38	1	0	0	0	1	41	92.70%
T.G	0	1	58	2	0	1	0	62	93.50%
A.L	1	0	0	38	1	0	2	42	90.50%
B.U	0	1	0	0	49	1	0	51	96.10%
W.B	2	0	1	0	1	50	0	54	92.60%
W.L	0	0	1	0	1	**0**	28	30	93.30%
Column total	61	40	62	40	52	54	31	340	
Producer's accuracy	93.40%	95%	93.54%	95%	96.10%	92.60%	90.30%		
Overall accuracy					93.50%				
Kappa coefficient					0.891				

Table 4 Land use/cover description

Land use/cover type	Description
Forest	Mixed forest with higher density of trees.
Light vegetation	Scattered trees, bush land dense shrubs.
Agricultural field	Land used for single crop, double crop/multi crop, fallow land.
Agricultural plantation	Mainly tea garden, horticulture plantation
Built up	Total area of the settlements, infrastructural development, industries, transportation, public utility
Water body	Including river, pond, tanks, water reservoirs, and water channels.
Waste land	Bare, exposed areas, and sandy areas.

Step2: Conversion from spectral radiance to at-satellite brightness temperatures

Emissivity corrections have applied to radiant temperature according to the land cover nature following Artis and Carnahan (1982).

$$T = \frac{K_2}{Ln\left(\frac{K_1}{L_\lambda} + 1\right)} - 273.15 \qquad (5)$$

where T represents at-satellite brightness temperature in Kelvin (K), $L\lambda$ represents at-satellite radiance in W/(m^2 sr μm), and K_1 and K_2 represent thermal calibration constant in W/(m^2 sr μm).

(For Landsat-5 TM, $K_1 = 607.76$ $K_2 = 1260.56$ for band 6, and For Landsat 8 OLI value of K_1 for band 10 and 11 are 774.8853 and 480.8883 respectively and K_2 for band 10 and 11 are 1321.0789 and 1201.1442 respectively. Values of K_2 and K_1 were obtained from metadata file.

The values of thermal constant for Landsat TM and Landsat OLI are then converted from Kelvin (K) to °C using the relation of $0\,^{\circ}$C equals 273.15 K. for better comprehension.

Step 3: Evaluation of land surface emissivity (E)

The above-derived temperature values are referenced to a black body. Therefore, spectral emissivity (E) corrections become necessary. These can be done according to the land cover nature (Snyder et al. 1998) and also by determining
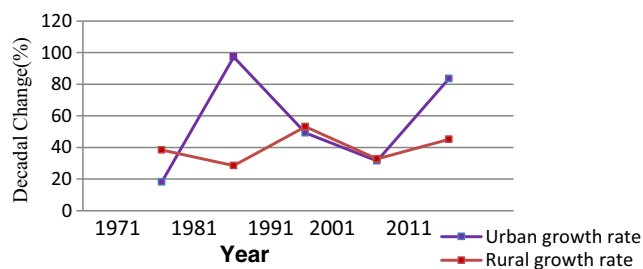
Fig. 3 Percentage change in decadal population in SJDA (1971–2011)

the corresponding emissivity values from the proportion of vegetation (Pv) values for each pixel.

$$E = 0.004 * P_V + 0.986 \qquad (6)$$

where proportion of vegetation (P_V) can be calculated as:

$$P_V = \{(NDVI - NDVI_{min})/(NDVI_{max} - NDVI_{min})\}^2 \qquad (7)$$

Step 4: Land surface temperature (LST)

The following equation is used to derive LST.

$$BT/1 + W * (BT/P) * Ln(E) \qquad (8)$$

where, BT represents the at-satellite brightness temperature, W is the wavelength of emitted radiance, $P = h*c/s$ (1.438 × 10 -2 m K), h is the Planck's constant (6.626 × 10 -34 Js), s is the Boltzmann constant (1.38 × 10 -23 J/K) and is the velocity of light (2.998 × 10 8 m/s).

Methodology for calculating spatial indices

Calculation of Normalized Difference Vegetation Index (NDVI)

To establish the correlation between LST with different spatial indices like NDVI (Normalized Difference Vegetation Index), NDWI (Normalized Difference Water Index), and NDBI (Normalized Difference Built Up Index) of the study area has been extracted by the following way.

Townshend and Justice (1986) method has been applied for extracting NDVI value.

$$NDVI = \frac{(NIRband - Rband)}{(NIR\ band + Rband)} \qquad (9)$$

where, NIR is the DN (digital number) value from the near infrared band and R is the DN value from the red band. The NDVI value ranges between 0 and 1. Values near to 0 indicate low vegetation cover and the value close to 1 indicates high density of vegetation.
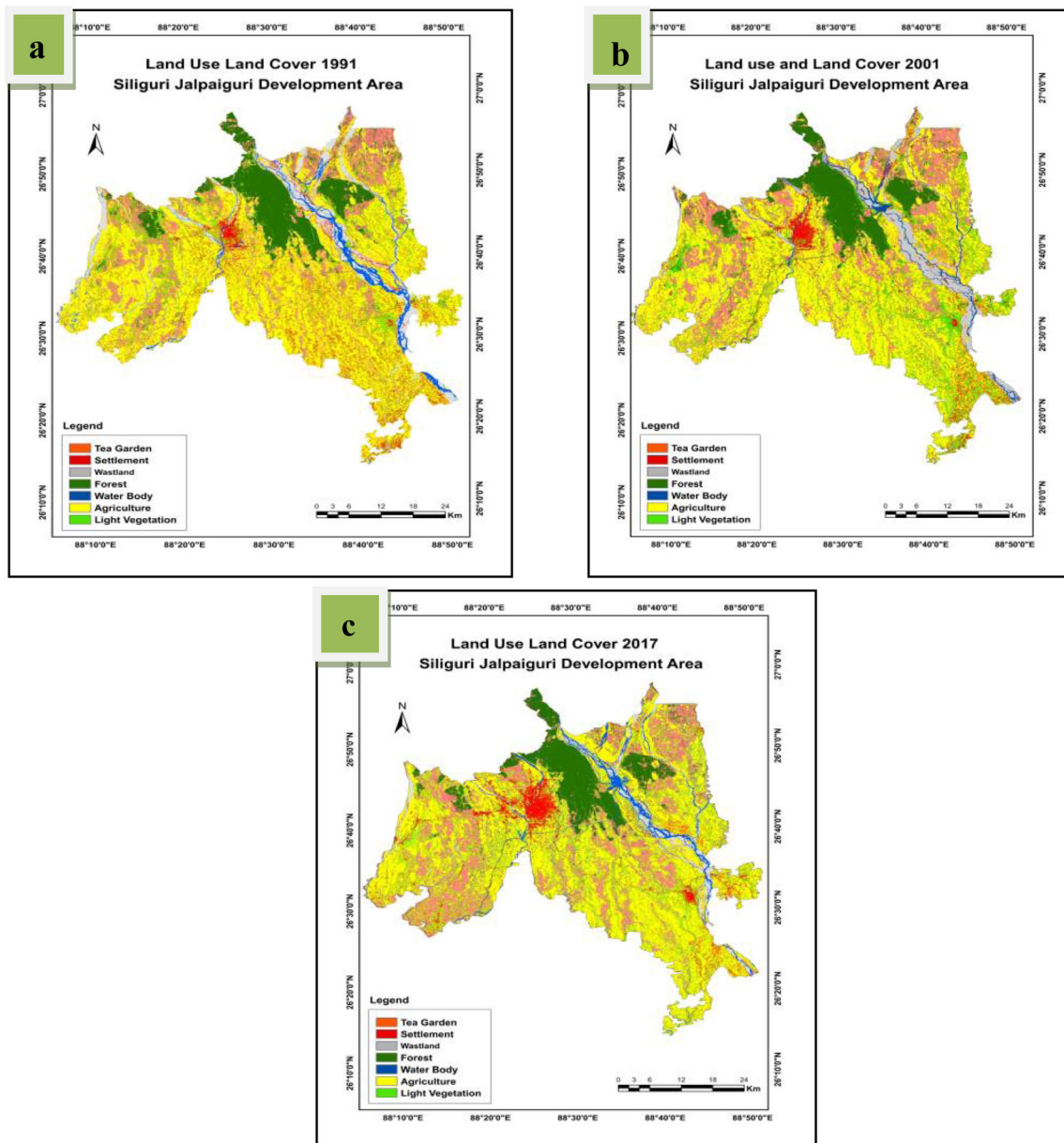
Fig. 4 Land use/land cover maps of SJDA. **a** 1991. **b** 2001. **c** 2017

Calculation of Normalized Difference Built up Index (NDBI)

NDBI is obtained by using the following formula (Zha et al. 2003) where the value closer to 1 indicates high density of built-up land.

$$NDBI = \frac{MIR\ band - NIR\ band}{MIR\ band + NIR\ band} \quad (10)$$

where, MIR is the DN value from the middle infrared band and NIR is the near infrared band.

Calculation of Modified Normalized Difference Water Index (MNDWI)

$$MNDWI = \frac{(Green\ band - NIR\ band)}{(Green\ band - NIR\ band)} \quad (11)$$

To eliminate the problem of inclusion of built-up area in NIR band-modified NDWI (MNDWI) is being applied (Gu et al. 2008), where, green means green band and NIR is the near-infrared band.

Table 5 Land use/land cover distribution of SJDA: 1991, 2001, and 2017

Land use type	Area (Km^2) (1991)	Percentage (%)	Area (Km^2) (2001)	Percentage (%)	Area (Km^2) (2017)	Percentage (%)
Forest	308.39	11.49	272.16	10.14	231.5	8.7
Light vegetation	332.28	12.38	282.89	10.54	237.27	8.84
Agricultural field	1187.87	44.63	1027.7	38.29	885.06	30.74
Tea garden	365.56	13.62	509.96	19	782.92	29.17
Built up	95.28	3.55	211.77	7.89	297.12	11.07
Water body	138.03	5.18	167.75	6.25	194.32	7.24
Waste land	269.89	10.13	215.79	8.04	117.56	4.38
Total	2684	100	2684	100	2684	100

Computed by author from image data extraction

After calculating the values of different spatial indices, output maps have been prepared to show spatial distribution of vegetation cover, built-up areas, water coverage over the time.

Statistical analysis and the relationship between LST and related indices

The distribution pattern of LST among different LULC types such as built-up area, vegetation cover, agricultural land, water bodies, and waste land, has been obtained along the projected profile lines. In order to show the relationship between LST and spatial indices, regression analysis is carried out with the values measured from selected sample points over the region. The correlation is determined from slopes of regression lines by fitting the trend line using Microsoft Excel.

Results and analysis

Accuracy assessment

The accuracies of classified land use land cover maps were assessed by verifying selected samples of each land cover classes with the help of ground truth data from Google archive images. Tables 2 and 3 display the results of accuracy assessment of post classification, i.e., the user's accuracy,

producer's accuracy, overall accuracy, and Kappa coefficient of classified LULC layers for the years 1991 and 2017. The post land use classification overall accuracy of 1991 and 2017 are 87.20% and 93.50% which indicates good accuracy results and effectiveness of the adopted classification technique (Tables 2 and 3).

Land use and land cover classification

Satellite images of three different years (1991, 2001, and 2017) have been compared to quantify the magnitude of LULC change in SJDA for last 26 years. Seven land use types were identified for obtaining the information of changes in land use pattern induced by growth of population (Table 4 and Fig. 3).

The state of land use and land cover in three temporal periods is provided in Table 5 and Fig. 4. In 1991, chief portion of land use has been given over to agricultural practice (44.63%) and intensive tea plantation (13.62%) which constitutes a major part in the region. Forest area is located primarily in the northern and north western hilly and Terai regions of the area. Forest tracts are mutated into new cultivable lands with growing population. The share of residential land use to total geographical land of the region is only 4% in 1991. This

Table 6 Land cover transition matrix of SJDA, from 2001 to 2017

Land use type	Forest	Light vegetation	Agricultural field	Waste land	Tea garden	Built up	Water body	Total 2001 (Km^2)
Forest	193 (70.95)	31.3 (11.50)	1.8 (0.65)	0.63 (0.23)	32 (11.75)	0.42 (0.14)	13.4 (4.940)	272.55
Light vegetation	18.41 (6.53)	151.34 (53.50)	1.41 (3.22)	5.78 (2.05)	63.2 (22.34)	30.17 (10.77)	12.15 (4.31)	282.46
Agricultural field	0.51 (0.05)	3.28 (0.031)	620.1 (60.63)	11.82 (1.15)	313.89 (30.54)	31.15 (3.06)	49.85 (4.95)	1030.6
Waste land	0	9.84 (4.56)	78.78 (36.51)	60.96 (28.25)	3.5 (1.63)	13.25 (6.14)	49.23 (23.83)	215.56
Tea garden	21.05 (4.13)	22.09 (2.15)	60.96 (11.96)	18.17 (3.57)	360.3 (70.72)	9.31 (1.83)	10.89 (2.14)	502.77
Built up	0	1.67 (0.79)	14.48 (6.84)	0.76 (0.36)	3.42 (1.62)	193.47 (91.34)	0.38 (0.18)	214.18
Water body	0	20.00 (11.92)	48.42 (28.86)	19.57 (12.86)	5.96 (3.57)	19.59 (11.73)	53.98 (30.95)	167.52
Total 2017 (Km^2)	232.93	239.12	825.8	117.68	782.28	297.36	189.88	2685.6

Computed by the author from image data extraction

Figures in the row cells depict the amount of former land cover contributed to the current land cover shows in columns. The diagonal figures in italic represent the unchanged area of LULC of each class during respective period. Values in parenthesis are the corresponding percentage values
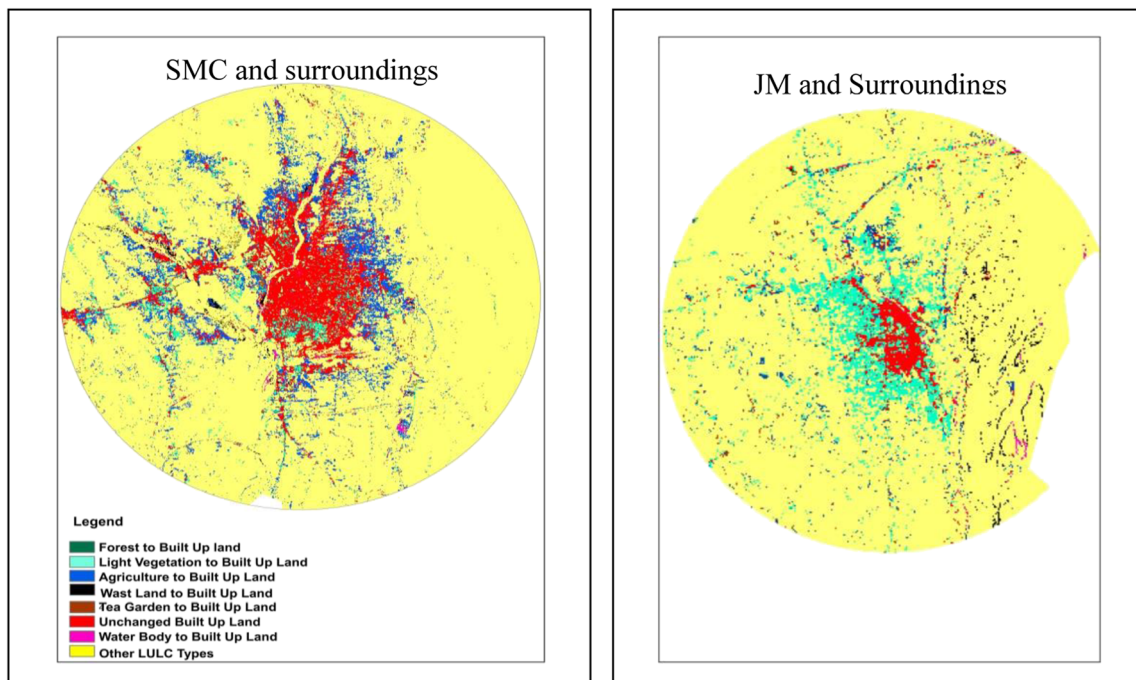
Fig. 5 Land transformation to residential area around the two major urban centers of SJDA from 2001 to 2017

indicates that the area has substantial land for accommodating growing population.

In 2001, the most prevalent land cover is agriculture though in 2001 agricultural land squeezed from 1187 to 1027 Km^2 due to transformation of agricultural land to mainly tea gardens. Tea plantation land in 2001 and 2017 also, had been accelerated from 19% in 2001 to 29.17% in 2017 of total land cover. Forest area reduced in coverage area, and light vegetation also remarkably decreased from 11% in 2001 to 8% in 2017 (Table 5 here).

In 2017 (Fig. 4c), again agricultural land decreased to 885 Km^2 sharing 30.74% land cover area, due to the trend associated with intensification of agricultural plantation and shifting occupational pattern of settlements from traditional forest settlement to plantation settlement. So the areas where the forests still survive are now more interspersed by numerous patches of tea gardens as well as cultivation. Due to the formation of reservoirs and channels, the water management system of the region was improved which reflected in rise of water coverage area from 1991 to 2017. Accelerating constructional land results in a huge decrease (56%) of waste land in last 26 years. The LULC maps displaying built-up area increased distinctly in coverage as the region has experienced very rapid growth
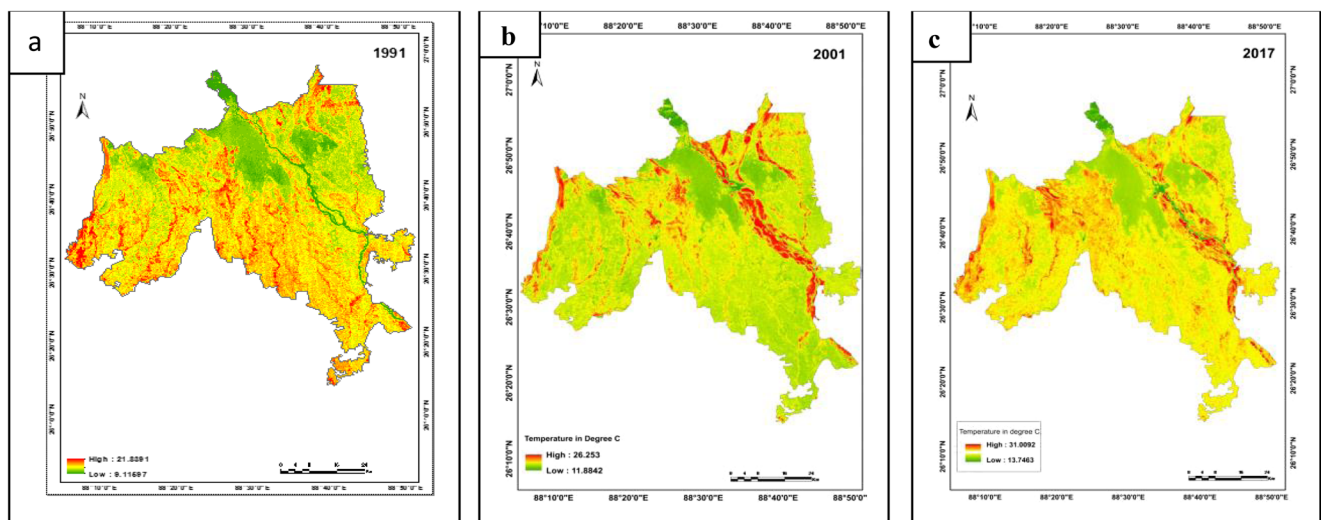

Fig. 6 Spatial distribution of land surface temperature in different temporal periods. **a** 1991. **b** 2001. **c** 2017

Table 7 Land use units wise changes in LST

Year wise temperature in °C	1991			2001			2017		
Land use types	Min.	Max.	Mean	Min.	Max.	Mean	Min.	Max.	Mean
Forest	9.12	19.34	14.75	11.88	23.25	17.49	15.16	26.93	20.83
Light vegetation	11.99	18.65	16.02	14.71	21.5	18.56	18.56	27.74	22.81
Agricultural land	10.57	21.1	16.7	13.31	26.25	19.57	17.73	30.59	23.82
Waste land	10.57	21.84	16.73	14.25	25.83	22.49	13.75	31.01	25.06
Tea garden	11.99	20.01	16.1	14.25	23.25	19.08	17.89	27.06	22.36
Built up	11.044	20.93	16.99	13.31	24.98	19.39	15.94	30.92	23.94
Water body	9.6	21.83	14.84	12.36	25.83	19.09	15.55	30.12	22.83

Computed by author with the help of ArcGIS

rate (122%) of built-up area from 95 to 211 Km² in between 1991 and 2001 (Fig. 4a–c).

Land conversion

Transition matrix between 2001 and 2017 has been produced to assess the current pattern of land cover change in the region. In between 2001 and 2017 (ref.Table 6), significant transition of wasteland (72.75%) to agricultural field, water body, and built-up area is found. Sixty-nine percent converted water body area was shared by agricultural field, waste land, and built-up area. Significant change is marked for agricultural land which mainly gained its land from waste land (36.51%), water body (28.86%), and light vegetation (3.22%). Tea garden area expanded at the expenses of agricultural field (30.54%), light vegetation (22.34%), and forest (12%). (Table 6).

Percent change of built-up area is 39% within the time span of 2001–2017, and this built-up area has increased significantly at the cost of the decrease of water body, light vegetation, and waste land. As the expansion in built-up land was predominantly in the areas immediately surrounding the core urban areas, 10-Km buffer zone around the center from Siliguri Municipal Corporation (SMC) and 5-Km buffer area from Jalpaiguri municipal (JM) area has taken to visualize land conversion dynamics clearly (Fig. 5). It is noted from

Table 8 Land surface temperature statistics of different temporal periods

Year	1991	2001	2017
Minimum °C	9.12	11.88	13.75
Maximum °C	21.84	26.25	31.01
Mean °C	16.3	19.3	23.94
SD	1.05	1.58	1.47
CV	6.44	8.19	6.38

Computed by the author from Landsat data with the help of Arc Gis

the land transform map of SMC and JM that in between 2001 and 2017, agricultural lands (37.35%), sparse vegetation (10.94%), water bodies (3.69%), and vacant land (2.86%) are more affected by residential expansion (Fig. 5).

From the analysis of 1991, 2001, and 2017 land use maps, it is evident that most of the areas in the region have undergone a transition in status from forest and vegetated area to extensively cultivated, plantation, and expanding residential land.

Impacts of land cover change

Change in land surface temperature distribution (LST)

Land surface temperature distribution maps of Siliguri Jalpaiguri Planning Area in different temporal periods have generated to present the change in LST distribution (Fig. 6 here). It is evident from the figures that LST values increased throughout the years from outskirts towards the inner urban areas. Figure 6 a) shows that in 1991 the lowest radiant temperature is 9.12 °C in dense hilly forest area in the northern part and the highest radiant temperature is 21.84 °C in the built-up area. For the year 2001, the radiant temperature ranges between 19.30 and 26.25 °C; the highest mean temperature is within built-up area, and the lowest temperature is within forest and water body bodies. However, the areas of sand deposits show high temperature because of high temperature reflectance. In 2017 (Fig. 6c), the highest temperature is increased to 31.1 °C clustered in the inner urban area. Table 7 depicts clear impression of the changes of LST over different land use units from 1991 to 2017. LST which is considerably increased over each land cover units specially, built-up land, sand deposition, and water body area has experienced 6.25 °C, 8.3 °C, and 7.99 °C increase of mean LST respectively. On average over 26 years of observation reveal almost 7 °C increase of mean LST in the study area (Tables 7 and 8).
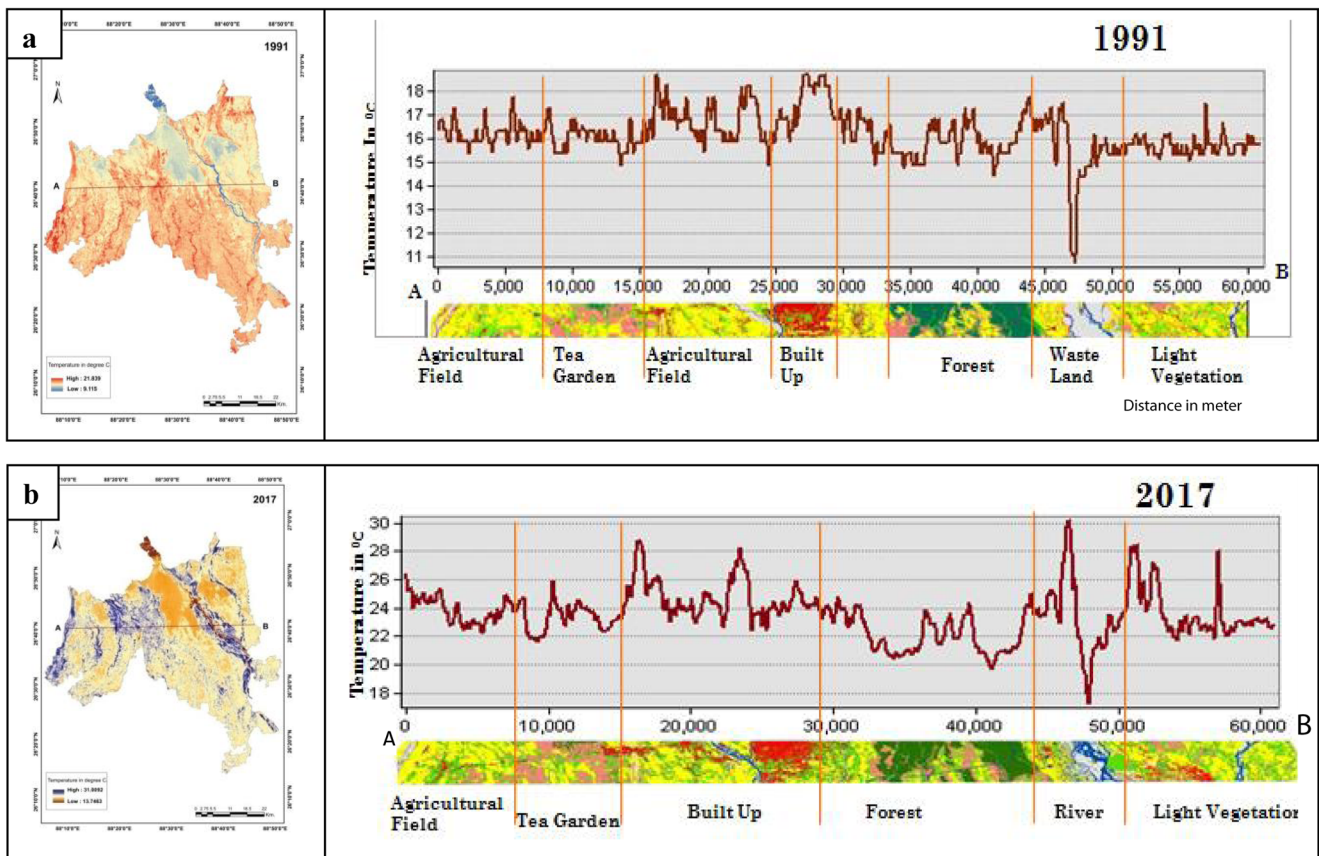
**Fig. 7** Comparison of LST profiles over different land cover types

Temperature distribution along LST transects profile by LULC types

Two profiles across (A-B) the same area and month (January) for two different years are generated to show the variations of land surface temperature in between 26 years. Basically, the spatial patterns of LST concentration highlight the change of

LULC distribution as there is close association between LST and LULC types (Fig. 7).

Comparison of change in distribution of temperature with different LULC types reveals in Fig. 7. The graph plotted in Fig. 7a shows highest land surface temperature value of 20.4 °C in built-up area in 1991. Temperature cross section profile gradually changes over different land cover areas. The

Fig. 8 Urban heat island profile
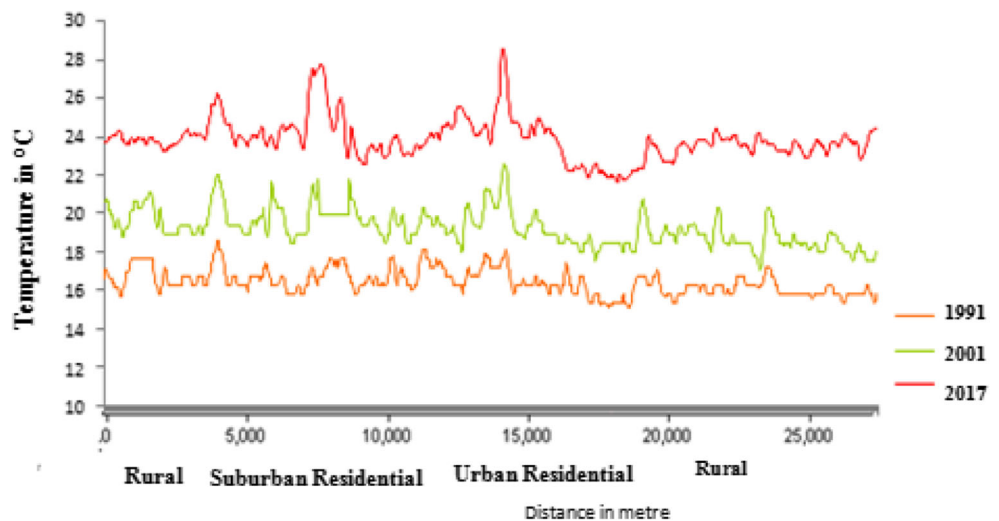
Table 9 Land surface temperature by residential land types

Residential land cover	1991	2001	2017
Urban	18.13 °C	22.5 °C	29.4 °C
Suburban	17.56 °C	21.8 °C	27.68 °C
Rural	16.17 °C	20.1 °C	24.6 °C
U-R temperature difference	1.96 °C	2.4 °C	4.8 °C

Table 10 Maximum, minimum, mean, S.D., and C.V of NDVI, NDBI, and MNDWI in study years

	Years	1991	2001	2017
NDVI	Minimum	− 1	− 1	− 0.15
	Maximum	0.58	0.056	0.51
	Mean	0.157	− 0.19	− 0.23
	SD	0.14	0.12	0.1
	CV	− 89.17	− 63.16	43.48
MNDWI	Minimum	− 0.68	− 1	− 0.45
	Maximum	1	0.71	0.19
	Mean	− 0.34	− 0.35	− 0.21
	SD	0.12	0.01	0.08
	CV	− 35.29	− 2.86	− 38.09
NDBI	Minimum	− 0.75	− 0.65	− 0.51
	Maximum	0.41	0.24	1
	Mean	− 0.37	− 0.35	− 0.19
	SD	0.07	0.07	0.12
	CV	− 18.92	− 20	− 63.16

surface temperature is much lower in forested area, and the lowest temperature acquired in the water body which is 11.2 °C. Surface temperature in tea garden area, agricultural field, scattered vegetated area shows moderate temperature ranges from 15 to 17.5 °C.

In 2017, Fig. 7b insights a different temperature statistics across the same profile. Temperature in the built-up surface rises to 28.5 °C though highest temperature acquired in sand deposited area because of high temperature absorption. Lowest temperature found in water body area is 17 °C. The temperature in forest, tea garden, and agricultural land is significantly lowered than built-up land which ranges between 20 and 26 °C. So the transect profiles clearly show that LST rises much high during 1991–2017 in different land cover category.

Urban temperature analysis

Special emphasis of the study has been given over to the analysis of urban land surface temperature profiles of SJDA. The changes of temperature in different temporal periods from core urban to periphery area along the profile covering Siliguri municipal corporation (SMC), its surrounding suburbs, and rural areas have been extracted (Fig. 8). The temperature of the core built-up areas of SMC is much higher than the areas located further away. Throughout the years, urban built-up area exhibits the highest surface temperature of 18.13 °C in1991, 22.5 °C in 2001, and accelerates to 29.4 °C in 2017. This implies rapid development of dense built-up surface such as stone, concrete, and metal constructions by replacing natural features as vegetation water body, which increases the

surface radiant temperature. The difference in derived radiant temperature between urban, sub urban, and rural residential areas has been summarized in Table 8. Nevertheless, the temperature difference clearly indicates the formation of Urban Heat Island (Fig. 8 and Table 9).

Figure 9 highlights the proportion of area within the 10-Km buffer zone around SMC, under different temperature zones and it is shifting from 1991 to 2017. A huge shifting of area under different temperature classes can be visualized within last 26 years. While in 1991, the largest proportion of area (47.96%) lied under the zone of 15.1–16.8 °C; in 2017, it is found that 70% area lie under the temperature of 20.64–24.05 °C, and 27% area lie under 24.5–27.49 °C (Fig. 9).

Analysis of spatial characteristics of NDVI, NDBI, and MNDWI

Vegetation cover maps have been prepared by calculating NDVI for the year 1991, 2001, and 2017. The descriptive

Fig. 9 Proportion of urban area under different temperature classes from 1991 to 2017
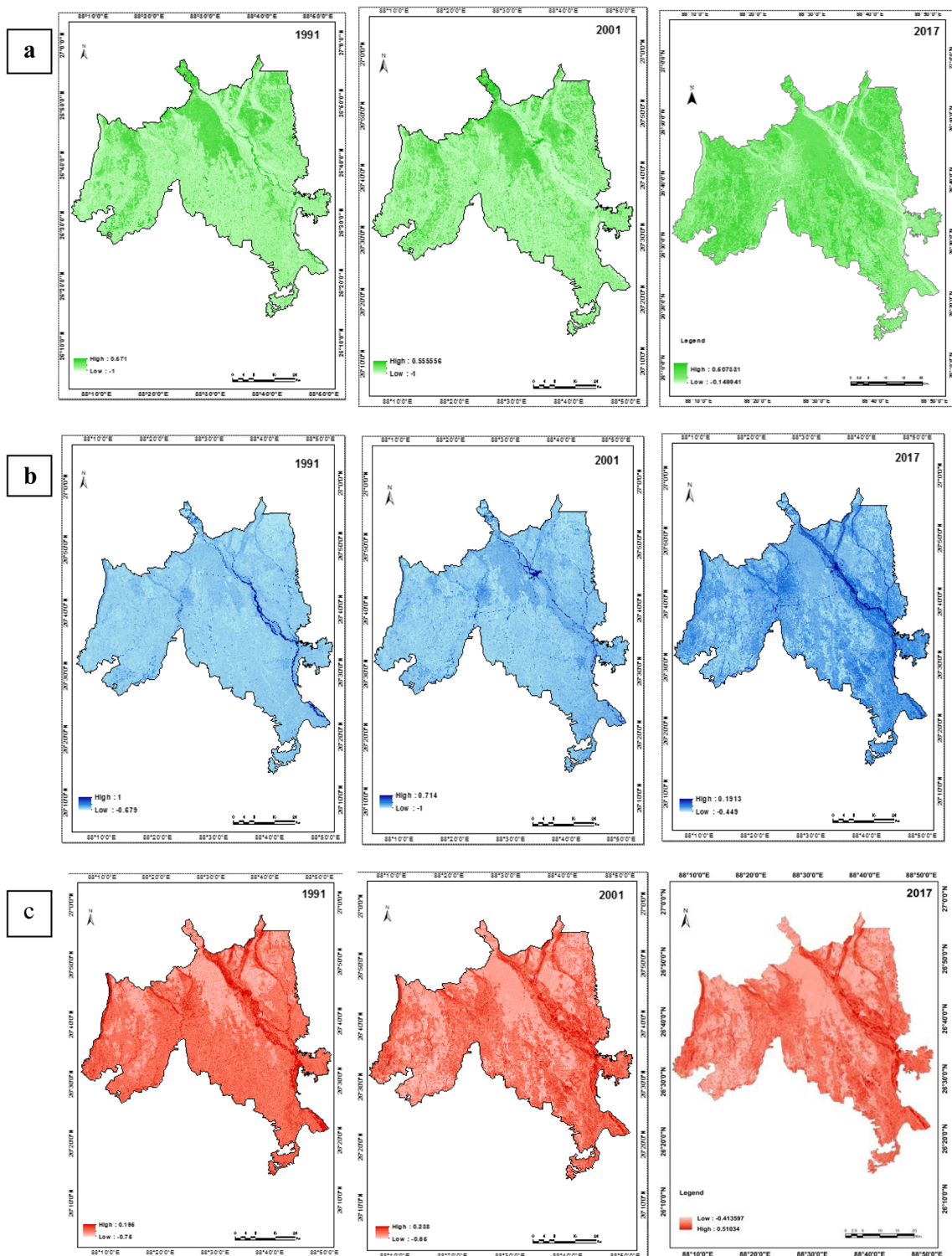
Fig. 10 Spatial distribution of **a** NDVI, **b** MNDWI, and **c** NDBI of different temporal periods

statistics of NDVI, NDBI, and NDWI through temporal periods are shown in Table 10. Coefficient of variation (CV) has been put to depict the relative dispersion of measured spatial indices for each study year.

The decrease in the vegetation growth coverage (scatter vegetation and forest) within the urban area can clearly be seen. Lower NDVI value was also located in water body areas. Higher NDVI values are observed in the middle

Fig. 11 Regression correlation between LST and **a** NDVI, **b** MNDWI, and **c** NDBI
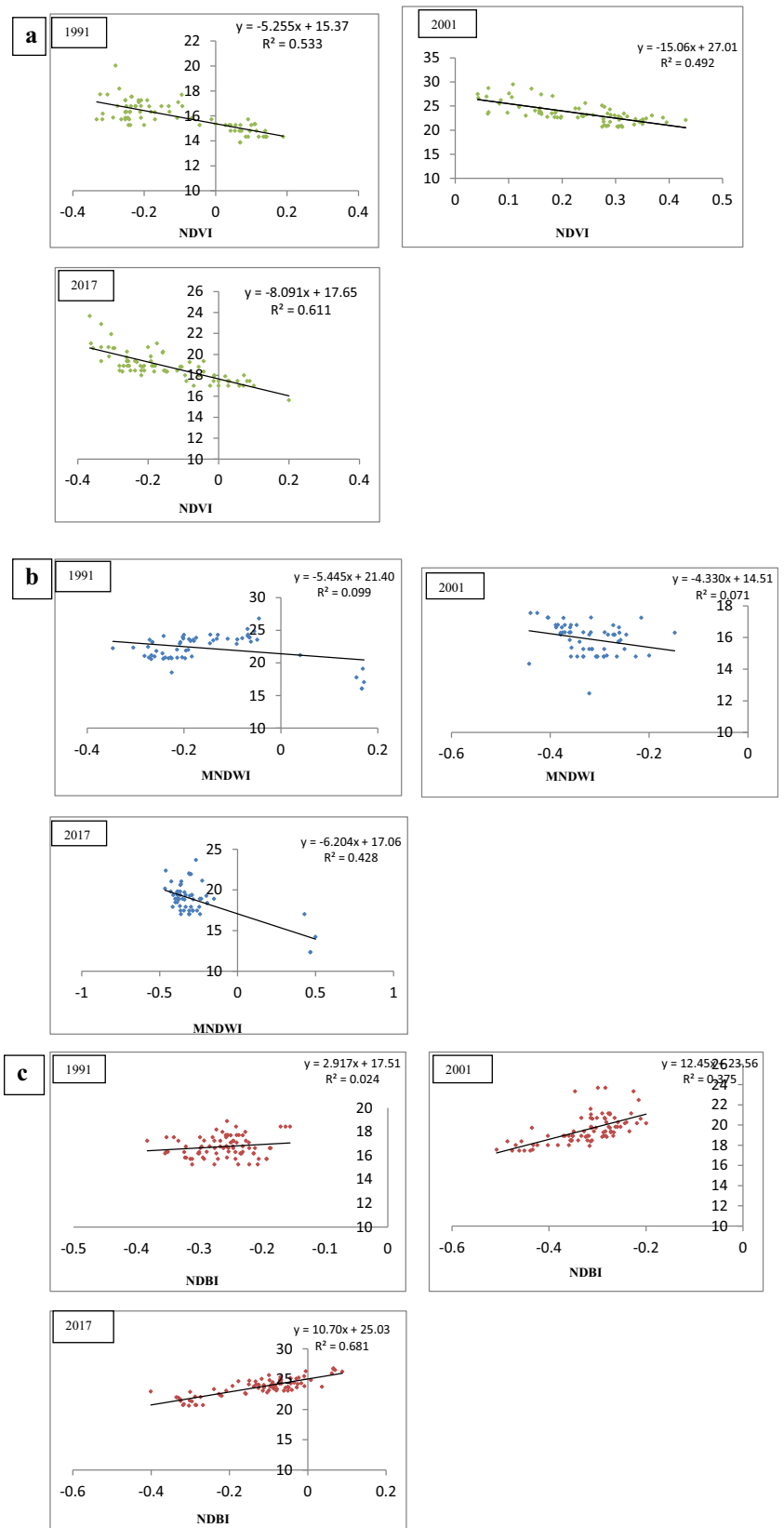
portion of dense forest area of the region. NDVI reflects an opposite picture of land surface temperature as NDVI value

increases hence LST value decreases. Vegetation cover highlights lowest mean NDVI value in 2017 with a value of −

0.23 and higher variation (43.48) of vegetation cover in 2017 (Fig. 10).

MNDWI pattern of the year 1991, 2001, and 2017 has extracted by using MNDWI index (Fig. 10b). There is significant change in the coverage of the water bodies as maximum MNDWI value decreases from 1 in 1991 to 0.19 in 2017. The main water body is river Teesta in the north eastern part of the region where MNDWI concentration is highest at the Teesta barrage. Presence of water bodies helps in reducing its own as well as surrounding temperature at some level (Table 10).

Built-up maps are generated by using NDBI (Normalized Difference Built up Index) to visualize built-up growth (Fig. 10c) of the area. High NDBI values are found in built-up land and vacant land of dense town areas. Maximum NDBI value remarkably increased due to land transformed to constructed land with industrial and commercial building, high rise residential building, facilities building, road, and transport communication. Hence high NDBI value can be visualized in built-up areas and other impervious areas, over the water bodies, and vegetation cover, NDBI values can be observed low.

Correlation between LST and LULC types

To obtain the relationship between LST and other spatial indices, 60 sample points are measured within the planning region during the study years. The extracted values of the selected parameters (i.e., LST, NDVI, NDBI, and NDWI) are put for regression model analysis. Specifically, the relationship between LST and different land use types was carried out by analyzing linear regression model for each land use respectively. Strong negative correlation (ref. Figure 11a) between surface temperature and vegetation cover can be found in the area where the value of R^2 (coefficient of determination), derived from the regression model, are 0.533, 0.49, and 0.61 for the year 1991, 2001, and 2017 respectively. The high value of R^2 in 2017 established the fact that vegetation plays vital roles to alleviate surface radiant temperature (Fig. 11).

Negative correlation has been depicted between LST and NDWI implying lower temperature in water body area and higher temperature in non water body areas. This relationship clearly emerged from the linear regression model where the high R^2 value is 0.43 in 2017 implying that water body helps in reducing LST.

Figure 11 c shows perfect positive relation between LST and NDBI. The R^2 value generated from the model is higher in 2017 which is 0.68. Such a high value of R^2 established the facts that increase in built up or impervious surface trapped the radiation that positively controls LST. Thus, it is emerged from the study that land surface temperature (LST) is sensitive to each land use type, hence can be used to detect land use/land cover changes.

Conclusions

The study arrives at the major findings that there is an evident change in the spatial pattern of land use to accommodate the dynamic growth of the planning region. Due to rapid population growth in the urban areas of SJDA, there are dramatic changes in the land use pattern. A huge amount of light vegetation and agricultural land has been cleared; open spaces and wetlands are transformed to urban construction land cover. The study has confirmed that land cover alteration has great impact on the environment in terms of land surface temperature and green space reduction. The study also puts in evidence the accelerating temperature difference between rural and urban which leads to the formation of urban heat islands. Vegetation cover within the urban environment has significant impacts on the distribution of the UHI as green space regulates the radiant surface temperature. High LST has been found at dense built-up urban land which triggered the UHI phenomenon of the study region.

One of the significant outputs of the study is the assessment and evaluation of different spatial indices based on LULC types over the years and plotting of regression onto spatial indices with respect to LST. The relation emerges as NDBI and LST were positive, and the correlations between MNDWI, NDVI, and LST were negative. This can be used to understand and monitor the spatial dynamics of the region based on LULC changes by urbanization. Therefore, comprehensive analysis of changing land use pattern and its effects driven by urbanization could provide an insight on proper land use planning to mitigate the UHI effects and provide ecological sustainability in the region.

References

Afzan Buyadi SN, Naim WM, Misn A (2013) Green spaces growth impact on the urban microclimate. Procedia Soc Behav Sci 105: 547–557. https://doi.org/10.1016/j.sbspro.2013.11.058

Artis DA, Carnahan WH (1982) Survey of emissivity variability in thermography of urban areas. Remote Sens Environ 12(4):313–329. https://doi.org/10.1016/0034-4257(82)90043-8

Ayanlade A, Howard MT (2019) Land surface temperature and heat fluxes over three cities in Niger Delta. J Afr Earth Sci 151:54–66. https://doi.org/10.1016/j.jafrearsci.2018.11.027

Bowler DE, Buyung-Ali L, Knight TM, Pullin AS (2010) Urban greening to cool towns and cities: a systematic review of the empirical evidence. Landsc Urban Plan 97:147–155. https://doi.org/10.1016/j.landurbplan.2010.05.006

Briassoulis H (2000) Land use change: theoretical and modeling approaches In S Loveridge (Ed), Web book of regional science. Regional Research Institute, West Virginia University

Carlson TN, Ripley DN (1997) On the relation between NDVI, fractional vegetation cover, and leaf area index. Remote Sens Environ 62(3): 241–252. https://doi.org/10.1016/S0034-4257(97)00104-1

Foody GM (1992) On the compensation for chance agreement in image classification accuracy assessment. Photogramm Eng Remote Sens 58:1459–1460

Gu Y, Hunt E, Wardlow B, Basara JB, Brown JF, Verdin JP (2008) Evaluation of NDVI and NDWI for vegetation drought monitoring using Oklahoma Mesonet soil moisture data. Geophys Res Lett 35: 1–5

Landsat Project Science Office (2002) Landsat 7 Science Data User's Handbook. URL: http://ltpwww.gsfc.nasa.gov/IAS/handbook/handbook_toc.html, Goddard Space Flight Center, NASA, Washington, DC (last date accessed: 10 September 2003)

Liu H, Weng Q (2008) Seasonal variations in the relationship between landscape pattern and land surface temperature in Indianapolis, USA. Environ Monit Assess 144(1–3):199–219. https://doi.org/10.1007/s10661-007-9979-5

Ma Z, Redmond RL (1995) Tau coefficients for accuracy assessment of classification of remote sensing data. Photogramm Eng Remote Sens 61(4):435–439

Mallick J, Rahman A (2012) Impact of population density on the surface temperature and micro-climate of Delhi. Curr Sci 102(12):1708–1713

Mohan M, Pathan SK, Narendrareddy K, Kandya A, Pandey S (2011) Dynamics of urbanization and its impact on land use/land cover: a case study of megacity Delhi. J Environ Prot 2:1274–1283

Mubea K, Menz G (2012) Monitoring land-use change in Nakuru (Kenya) using multi-sensor satellite data. Adv Remote Sens 1:74–84. https://doi.org/10.4236/ars.2012.13008

Nkeki FN (2016) Spatio-temporal analysis of land use transition and urban growth characterization in Benin metropolitan region, Nigeria. Remote Sens Appl Soc Environ 4:119–137. https://doi.org/10.1016/j.rsase.2016.08.002

Purevdorj TS, Tateishi R, Ishiyama T, Honda Y (1998) Relationships between percent vegetation cover and vegetation indices. Int J Remote Sens 19(18):3519–3535. https://doi.org/10.1080/014311698213795

Ramachandra TV, Aithal BH, Durgappa SD (2012) Land surface temperature analysis in an urbanizing landscape through multi-resolution data. J Space Sci Technol 1(1):1–10

Snyder WC, Wan Z, Zhang Y, Feng YZ (1998) Classification-based emissivity for land surface temperature measurement from space. Int J Remote Sens 19(14):2753–2774

Sobrino JA, Jiménez-Muñoz JC, Paolini L, Jime JC (2004) Land surface temperature retrieval from LANDSAT TM 5. Remote Sens Environ 90(4):434–440. https://doi.org/10.1016/j.rse.2004.02.003

Townshend JR, Justice CO (1986) Analysis of the dynamics of African vegetation using the normalized difference vegetation index. Int J Remote Sens 7(11):1435–1445. https://doi.org/10.1080/01431168608948946

Turner BL, Meyer WB, Skole DL (1994) Global land-use/land-cover change: towards an integrated study. Ambio 23(1):91–95 http://www.jstor.org/stable/4314168

Weng Q (2001) A remote sensing–GIS evaluation of urban expansion and its impact on surface temperature in the Zhujiang Delta, China. Int J Remote Sens 22(10):1999–2014. https://doi.org/10.1080/713860788

Weng Q (2002) Land use change analysis in the Zhujiang delta of China using satellite remote sensing, GIS and stochastic modelling. J Environ Manag 64(3):273–284. https://doi.org/10.1006/jema.2001.0509

Xiao R, Ouyang Z, Wang X, Li W (2002) Detecting and analyzing urban heat island and patterns in Beijing, China. Research Center for Eco-Environmental Sciences, Chinese Academy of Sciences, Beijing 100085, China

Xu H (2006) Modification of normalised difference water index (NDWI) to enhance open water features in remotely sensed imagery. Int J Remote Sens 27(14):3025–3033. https://doi.org/10.1080/01431160600589179

Zha Y, Gao J, Ni A (2003) Use of normalized difference built-up index in automatically mapping urban areas from TM imagery. Int J Remote Sens 24(3):583–594. https://doi.org/10.1080/01431160304987